THE ASTROPHYSICAL JOURNAL, 484:487–498, 1997 July 20

THEORETICAL AND LABORATORY STUDIES ON THE INTERACTION OF COSMIC-RAY PARTICLES WITH INTERSTELLAR ICES. II. FORMATION OF ATOMIC AND MOLECULAR HYDROGEN IN FROZEN ORGANIC MOLECULES

R. I. KAISER,[1] G. EICH, A. GABRYSCH, AND K. ROESSLER
Institut für Nuklearchemie, Forschungszentrum Jülich, 52425 Jülich, Germany
Received 1996 September 24; accepted 1997 February 7

ABSTRACT

Methane ices are irradiated at 4×10^{-10} mbar at temperatures between 10 and 50 K with 9.0 MeV α-particles and 7.3 MeV protons to elucidate the formation of atomic as well as molecular hydrogen via interaction of Galactic cosmic-ray particles with extraterrestrial organic ices. Theoretical calculations focus on computer simulations of ion-induced collision cascades in irradiated targets. Our data reveal that more than 99% of the energy is transferred via inelastic interactions to the electronic system of the target to form electronically excited CH_4 molecules decomposing to a CH_3--H radical pair. Two H atoms recombine in a diffusion limited step to H_2. Further, secondary dissociation of CH_3 to H and CH_2 contributes to H production. To a minor amount, implanted ions generate C and H knock-on atoms via elastic encounters which abstract hydrogen atoms or insert into chemical bonds (carbon atoms only). Fourier transform infrared spectroscopy (FTIR) and quadrupole mass spectrometry (QMS) analyses indicate that if these energy-loss processes accumulate up to $6 \pm 3\%$ H atoms in the CH_4 target, more than 90% of the ice is released in an explosive ejection into the gas phase. This mechanism represents a powerful pathway to supply newly formed molecules from interstellar grains back to the gas phase of the interstellar medium even at temperatures as low as 10 K.

Subject headings: atomic processes — cosmic rays — ISM: molecules — methods: laboratory — molecular processes

1. INTRODUCTION

Molecular hydrogen H_2 is the most abundant molecule in the interstellar medium (ISM). It is generally presumed that besides the dissociative recombination in the gas phase,

$$H^- + H \rightarrow H_2 + e^- , \quad (1)$$

recombination of two physi-/chemisorbed hydrogen atoms on interstellar grains via tunneling resembles *the* central H_2 source since a radiative association in the gas phase cannot get rid of the 4.5 eV bond energy via photon emission (Smuluchowski 1981; Tielens & Allamandola 1987; Hauge & Stovneng 1989),

$$2H \rightarrow H_2 . \quad (2)$$

The excess energy of this process is either dissipated via photons to the grain itself and/or released as kinetic energy of the H_2 molecule in the gas phase. A collisional stabilization of any internally excited gaseous H_2 molecule formed via reaction (2) can be dismissed when we consider lifetimes of interstellar molecules as well as clouds of 10^6–10^7 yr (compared to the timescale of a three-body reaction of 10^9 yr) (Becker, Hong, & Hong 1974). Besides grain-surface chemistry, UV (Sandford & Allamandola 1993; Bhattacharya & Willard 1982; Romani & Atreya 1988) and Galactic cosmic-ray processing of interstellar ices, such as CH_4/H_2O mixtures, are said to contribute to interstellar H_2 production (Pironello 1991; Johnson, Brown, & Lanzerotti 1983; Johnson 1996; Pironello & Averna 1988; Pironello et al. 1988, p. 287; Brown et al. 1987). Upon irradiation of solid CH_4 with 1.5 MeV protons and α-particles, for example, Brown et al. (1987) observed a delayed emission of molecular hydrogen as soon as a critical fluence of about 10^{14} cm^{-2} had been accumulated. Likewise, ion implantation into isotopically mixed D_2O/CH_4 targets reveals an HD release monitored via quadrupole mass spectrometer. However, detailed physicochemical mechanisms leading to H as well as H_2 in solids during ion irradiation of frosts are still elusive but essential to understand cosmic-ray–induced H_2 production in interstellar and planetary ices.

This paper is part of an ongoing project to investigate the chemical and physical effect of Galactic cosmic-ray MeV ion interaction with frozen organic samples. The objectives of our investigations are to focus on *deliberate model compounds* and to establish *a mechanistic model* before extending our studies to astrophysically relevant interstellar grain composita. The choice of MeV particles in our experiments characterizes the flux distribution maximum of Galactic cosmic-ray particles peaking at about 8–15 MeV (see discussion in Kaiser & Roessler 1997). Paper I of this series established a model to form polycyclic aromatic hydrocarbons (PAHs) in interstellar ices at temperatures as low as 10 K (Kaiser & Roessler 1997). Here we elucidate fundamental mechanisms based on laboratory and theoretical studies on the interaction of cosmic-ray particles with the simplest alkane, CH_4 (methane), in extraterrestrial ices to generate atomic and molecular hydrogen. Mechanisms are elucidated by (1) increasing the absorbed energy per target molecule, dose D, to 150 eV, (2) probing reactions of suprathermal (1–10 eV) atoms initiated by knock-on particles in the collision cascades, and (3) elucidating diffusion-limited chemistry of atoms, and CH, CH_2, as well as CH_3 radicals via substitution of CH_4 by CD_4, and addition of O_2 as a radical scavenger. CH_4/CD_4 mixtures are irradiated to distinguish between inter- and intramolecular reactions, whereas $^{13}CH_4$ targets are selected to verify on-line and in situ Fourier transform infrared (FTIR) spectroscopy and quadrupole mass spectrometry (QMS) data. Our experi-

[1] Present address: Department of Chemistry, University of California, Berkeley, CA 94720; kaiser@leea.cchem.berkeley.edu.

mental doses represent equivalent irradiation by the interstellar cosmic-ray particle field of $\approx 1 \times 10^9$ yr.

2. EXPERIMENTAL APPROACH AND COMPUTATIONAL MODEL

The experimental setup is described earlier in detail (Kaiser, Gabrysch, & Roessler 1995a; Kaiser & Roessler 1997). Briefly, all experiments are performed in an ultra high vacuum (UHV) chamber at about 4×10^{-10} mbar. Ice layers are condensed onto a 10 K silver wafer and cycled after the initial deposition to 50 K and back to 10 K to prepare a well-defined low-temperature modification 1 (see Tables 1 and 2). The targets are irradiated with 9.0 MeV α-particles at fluxes of $\phi(\alpha) = 127$ nA cm^{-2} isothermally at 10 K in the low-temperature (LT) experiment or heated during the irradiation to 50 K in the high-temperature (HT) experiment. The solid state is monitored on line and in situ with a Fourier transform infrared (FTIR) spectrometer (4000–400 cm^{-1}; NICOLET) in absorption-reflection, whereas a quadrupole mass spectrometer (QMS) probes the gas phase; data processing is performed via matrix interval algebra to include experimental uncertainties of the relative gas concentrations (Kaiser et al. 1995b). Physical processes triggered by the ion implantation into a CH_4 target are simulated with the MARLOWE program (Robinson 1992; Roessler 1992) extended for quantum mechanical and relativistic treatments of our MeV ions (Kaiser & Roessler 1997). This code calculates elastic and inelastic energy transfers from an impinging particle to the target atom(s) of the condensed hydrocarbon ices.

3. RESULTS

3.1. *Computer Simulations*

The MARLOWE calculations show that 9 MeV α-particles and protons transfer more than 99% of the energy in inelastic encounters to the electronic system of the CH_4 target. This energy transfer leads to electronic excitation, ionization, and/or C-H bond cleavage in a single CH_4 molecule to methyl radicals, CH_3, and atomic hydrogen:

$$CH_4 \rightarrow H + CH_3 \, . \quad (3)$$

This process was found to dominate even in γ-ray irradiated samples at 77 K (Trakhtenberg & Milikh 1982; Grigorev et al. 1988) inducing a diffusion of free valences in the solid state via H abstraction from a second methane molecule to form H_2, and a second CH_3 radical. The ultimate outcome was reflected in an upper radical concentration before neighboring radical recombination took over.

The remaining less than 1% kinetic energy of the primary projectile is released via elastic collisions igniting collision cascades with energies of the knock-on particles up to 10 keV. Averaging over 10^4 simulated cascades, we find total numbers of 0.22 ± 0.04 H/0.07 ± 0.02 C (7.3 MeV H^+) and 3.17 ± 0.52 H/1.15 ± 0.25 C (9.0 MeV α) per impinging MeV particle in a 5 μm CH_4 target. Some collision cascades show an alignment effect, induced if a heavy particle (here: carbon atoms) knocks out light hydrogen atoms which themselves are pushed in front of the recoiling carbon atom (see Fig. 1; Roessler 1992). Further, our calculations depict a virtual zero sputtering yield of less than 0.3% of the target. The suprathermal H atoms can abstract a second H atom from a single methane molecule via equation (4),

$$H + CH_4 \rightarrow CH_3 + H_2 \, , \quad (4)$$

whereas knock-on carbon atoms insert via equations (5) and (6) to react to atomic and/or molecular hydrogen (Kaiser & Roessler 1997):

$$H\text{-}CH_3(X\,^1A_1) + C(^3P_j) \rightarrow [H\text{-}C\text{-}CH_3]^3 \rightarrow 2H(^2S_{1/2}) + C_2H_2(X\,^1\Sigma_g^+) \, , \quad (5)$$

$$H\text{-}CH_3(X\,^1A_1) + C(^1D_2) \rightarrow [H\text{-}C\text{-}CH_3]^1 \rightarrow H_2(X\,^1\Sigma_g^+) + C_2H_2(X\,^1\Sigma_g^+) \, . \quad (6)$$

TABLE 1

COMPILATION OF IRRADIATION EXPERIMENTS AND PARAMETERS

Target	Temperature	Layer Thickness (μm)	Ion	Wafer Temperature (K)	Irradiation Time (minutes)	Dose (eV)
$^{13}CH_4$	LT	4.0 ± 0.4	α	9.9 ± 0.2	60	29 ± 3
$^{13}CH_4$	HT	4.1 ± 0.4	α	10.4 ± 0.4	60	30 ± 5
CD_4	LT	5.5 ± 1.5	α	9.8 ± 0.1	60	30 ± 4
CD_4	HT	6.5 ± 0.9	α	9.7 ± 0.1	60	29 ± 4
CH_4	LT	4.3 ± 0.5	α	9.1 ± 0.1	60	29 ± 2
CH_4	LT	4.0 ± 0.4	p	9.6 ± 0.1	336	28 ± 3
CH_4/O_2 1%–2%.....	LT	6.9 ± 0.7	α	11.0 ± 0.5	60	28 ± 5

TABLE 2

CRYSTALLOGRAPHIC PARAMETERS OF IRRADIATED ICES

Target	Modification	Phase Change Temperature (K)	Density (g cm^{-3})	Space Group	Lattice Constant (Å)
$^{12}CH_4$.....	II	13.9	0.53	Fm3c[a]	5.84
CD_4	II	24.4	0.674	Fm3c[a]	5.84
C_2H_4	II	20.0	0.81	Im3m[a]	?
C_2H_2	II	135	0.826	Acam[b]	$a = 6.21$, $b = 6.01$, $c = 5.6$

[a] Lattice constant of one octant.
[b] Lattice constant of one unit cell.

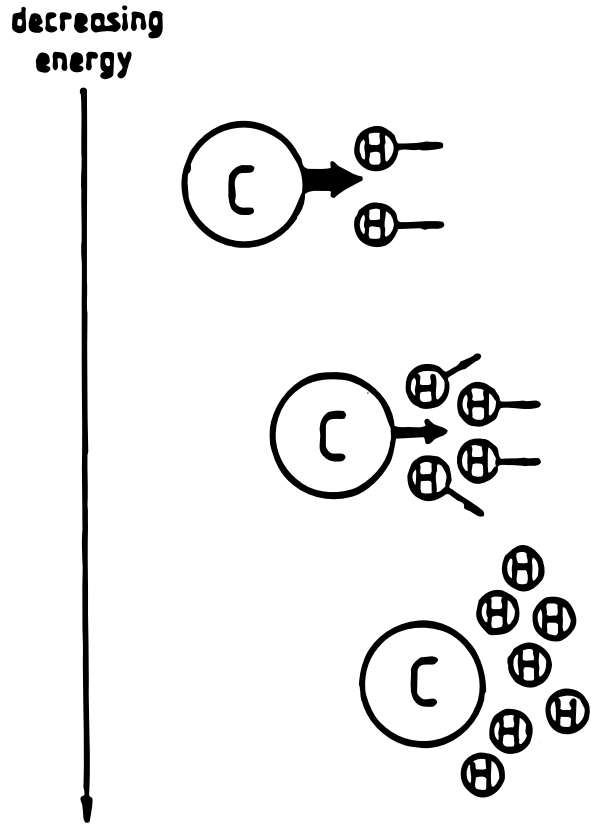

FIG. 1.—Schematic presentation of the development of aligned cascades.

3.2. *Quadrupole-Mass Spectrometry*

Since the CH_4 parent molecules and reaction products fragment to H_2 in the ionizer of the quadrupole mass spectrometer as well, different molecular species add the mass to charge ratio (m/e) of, e.g., 2 (H_2). Therefore, we must perform the raw data processing via matrix interval algebra to discriminate the contribution to $m/e = 2$ between H_2 formed upon ion irradiation experiments and the fragmentation of higher molecular products in the ionizer (Kaiser et al. 1995). m/e-ratios are chosen to result in an inhomogeneous system of linear equations including the measured ion current (right-hand vector), partial pressures (unknown quantity), and calibration factors of fragments of individual gaseous species determined in separate experiments. Since all quantities are provided with experimental errors, matrix interval arithmetic (i.e., an IBM high-accuracy arithmetic subroutine defining experimental uncertainties as intervals) is incorporated in the computations to extract individual calibrated components of gas mixtures. This procedure yields the contribution of $m/e = 2$ solely from synthesized H_2 molecules.

3.2.1. $^{13}CH_4$ *and* CD_4 *Targets*

3.2.1.1. 10 K Experiments

Figure 2 shows the temporal profile of the D_2/H_2 signal during the actual irradiation ($t = 0$ to beam off), a 60 minute equilibration period starting at "beam off," and the final target heating to 293 K. During all ion bombardments at 10 K (Figs. 2*a*, 2*b*, 2*e*, and 2*f*), the H_2/D_2 profiles rise linearly in the first 30 minutes and start leveling off as the irradiation time rises. These patterns correlate with theoretical calculations of Trakhtenberg & Milikh (1982) and Gregorev et al. (1988), indicating an upper limit of the radical concentration upon irradiation exposure. Integrating the H_2/D_2 profile of the low-dose irradiation from $t = 0$ to the end of the irradiation and correcting for the pumping speed (Figs. 2*a*–2*b*), we find a H_2 to D_2 ratio of 6 ± 2. These results very likely suggest an isotopic effect based on the enhanced diffusion constant k_D of H versus D of $k_D(H)/k_D(D) = 2^{1/2} = 14$. Upon annealing the target, Figures 2*c* and 2*d* clearly indicate a rising H_2/D_2 signal with increasing temperature reaching a maximum after 7 hr at 55 K when the CH_4 and CD_4 matrices have sublimed completely. Our data verify that the methane targets still store atomic and/or molecular hydrogen.

Radiation doses up to 145 eV induce pressure shocks (hereafter: explosions) rising the total pressure up to 7 orders of magnitude (see Figs. 2*e* and 2*f*). This process releases up to 90% of the molecules of the solid target into the gas phase as monitored via FTIR spectroscopy (see § 3.2.2). Since the energy loss of the MeV particles is dominated by inelastic processes leading to H and CH_3 formation (see § 3.1), these radicals are expected to play a key role in the mechanism to the pressure shock. The proof is even stronger if we compare these findings with the CH_4/O_2 (1% O_2) system (§ 3.2.3). Here, no explosion was monitored, and H_2 formation could not be verified at all. Therefore, mobile radicals are expected to be trapped in the CH_4/O_2 to inhibit the explosion. The FTIR studies will reveal the nature of these mobile species.

3.2.1.2. 10 K–50 K–10 K Experiments

In contrast to the 10 K experiments, the H_2/D_2 released during the irradiation phase at 50 K rises steeply and increases by about 4 orders of magnitude as a result of the enhanced diffusion coefficient of H/D at 50 K versus 10 K (see Figs 2*c* and 2*e*). This temperature dependence indicates that the dominant formation of H_2/D_2 is diffusion limited since suprathermal processes depict no temperature dependence of the production yield. The enhanced temperature reduces the capability of the methane target to store atomic as well as molecular hydrogen: during the annealing phase to 293 K, the H_2/D_2 signal is lower by about 2–3 orders of magnitude compared to the 10 K system.

3.2.2. CH_4/CD_4 *Targets*

During the 10 K α-particle irradiation, the mass spectrometer detects only the signal of reactant molecules at $m/e = 20$, 18, 16, 14, 12, 4 (CD_α; $x = 0.4$; D_2) and at $m/e = 16$, 15, 14, 13, 12, 2 (CH_x; $x = 0.4$; H_2) as well as the HD product (Fig. 3). The identification of HD at $m/e = 3$ verifies the existence of atomic H/D inside the solid target recombining via equation 7:

$$H + D \rightarrow HD\ . \tag{7}$$

3.2.3. CH_4/O_2 *Targets*

In strong contrast to the CH_4 targets, no H_2 could be probed in these experiments. However, since atomic hydrogen is definitely produced upon inelastic energy transfer to CH_4 molecules (§§ 3.1, 3.2.1, and 3.2.2), H atoms formed in situ must be trapped chemically in the solid target. Further, pressure shocks probed in 10 K experiments of CH_4 as well as CD_4 are completely absent. Therefore, for 1% O_2 admixture exhibits a profound effect on our experimental results and suggests that O_2 molecules and H/D atoms on the one

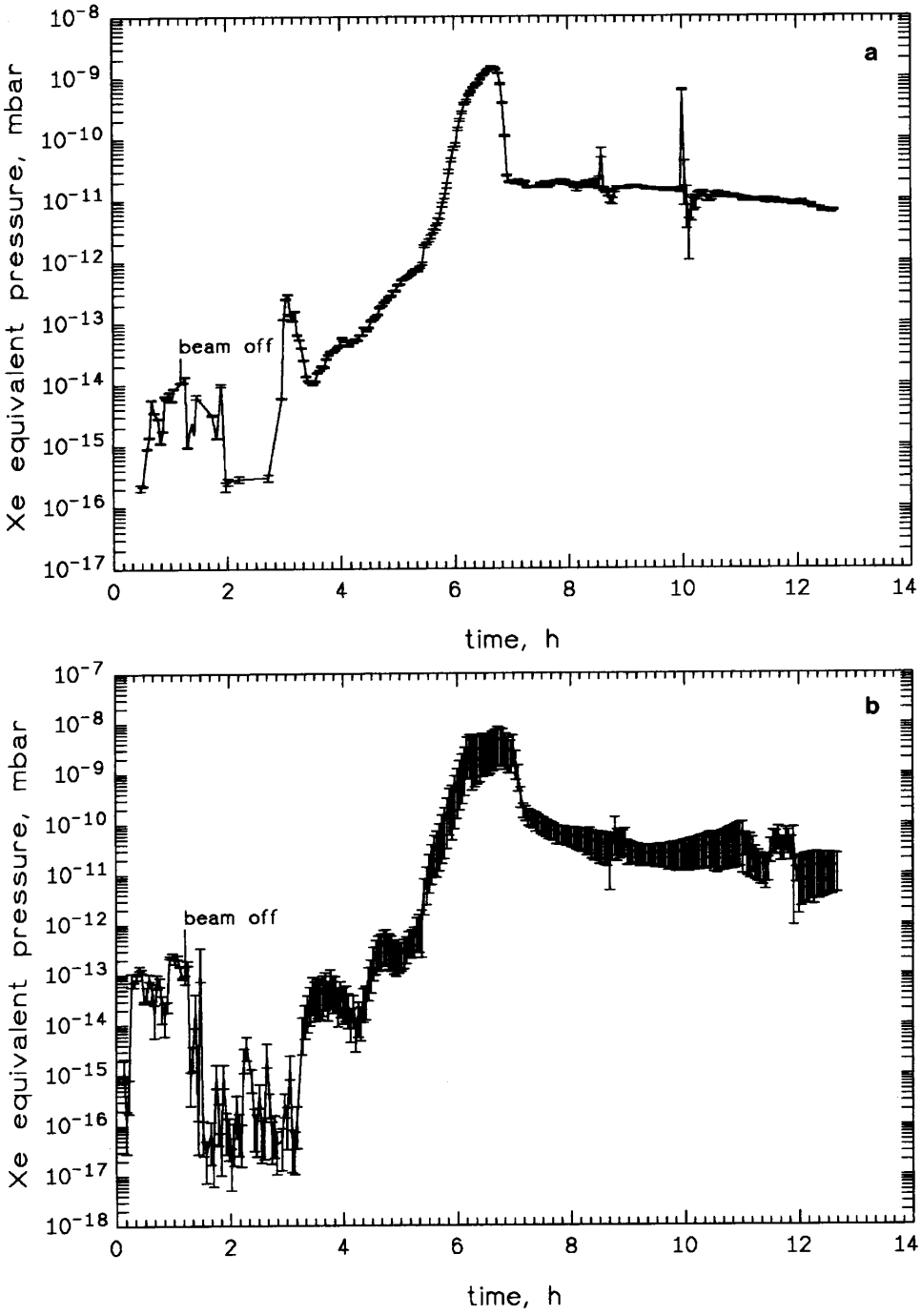

FIG. 2.—Temporal profiles of H_2/D_2 development upon 9 MeV α-particle ion irradiation as calculated via matrix interval algebra (*a*) CD_4, 10 K, 30 ± 4 eV; (*b*) $^{13}CH_4$, 10 K, 29 ± 3 eV; (*c*) CD_4, 50 K, 29 ± 4; (*d*) $^{13}CH_4$, 50 K, 30 ± 5 eV; (*e*) CD_4, 10 K, 144 ± 26 eV; (*f*) $^{13}CH_4$, 10 K, 145 ± 18.

hand, and the inhibited pressure shocks/missing H_2 synthesis on the otherhand, are strongly correlated.

3.3. *Fourier Transform Infrared Spectroscopy (FTIR)*

The FTIR spectra reveal supplementary information on formation of atomic and molecular hydrogen. Specifically, we (1) investigate the degradation of CH_4/CD_4 molecules to CH_3/CD_3 and CH_2/CD_2 radicals, (2) determine the fate of H and CH_3 in CH_4/O_2 experiments, and (3) elucidate the mechanism leading to target explosions at 10 K.

3.3.1. CH_4/CD_4 *Targets*

Besides identification of isotopically pure radicals CH_2, CH_3, CD_2, and CD_3, mixed species are prominent tracers for recombination and H-D-exchange reactions at 10 K. FTIR spectra depict absorption of CH_2D (563 cm^{-1}), CHD_2 (513 cm^{-1}), and CHD_3 (998.2 cm^{-1}; 1284.7 cm^{-1}) as the dose rises (Fig. 4). Most important, CH_3 and CD_3 absorption appear instantaneously in the first IR spectra averaged over 6 minutes irradiation time, whereas CH_2 and CD_2 patterns depict a signal delayed by 6 minutes. These data strongly suggest that both carbene radicals are formed in secondary processes as soon as a methyl radical concentration high enough for reactions (8) and (9) is reached. The initial linear formation rate of methyl radicals levels off with

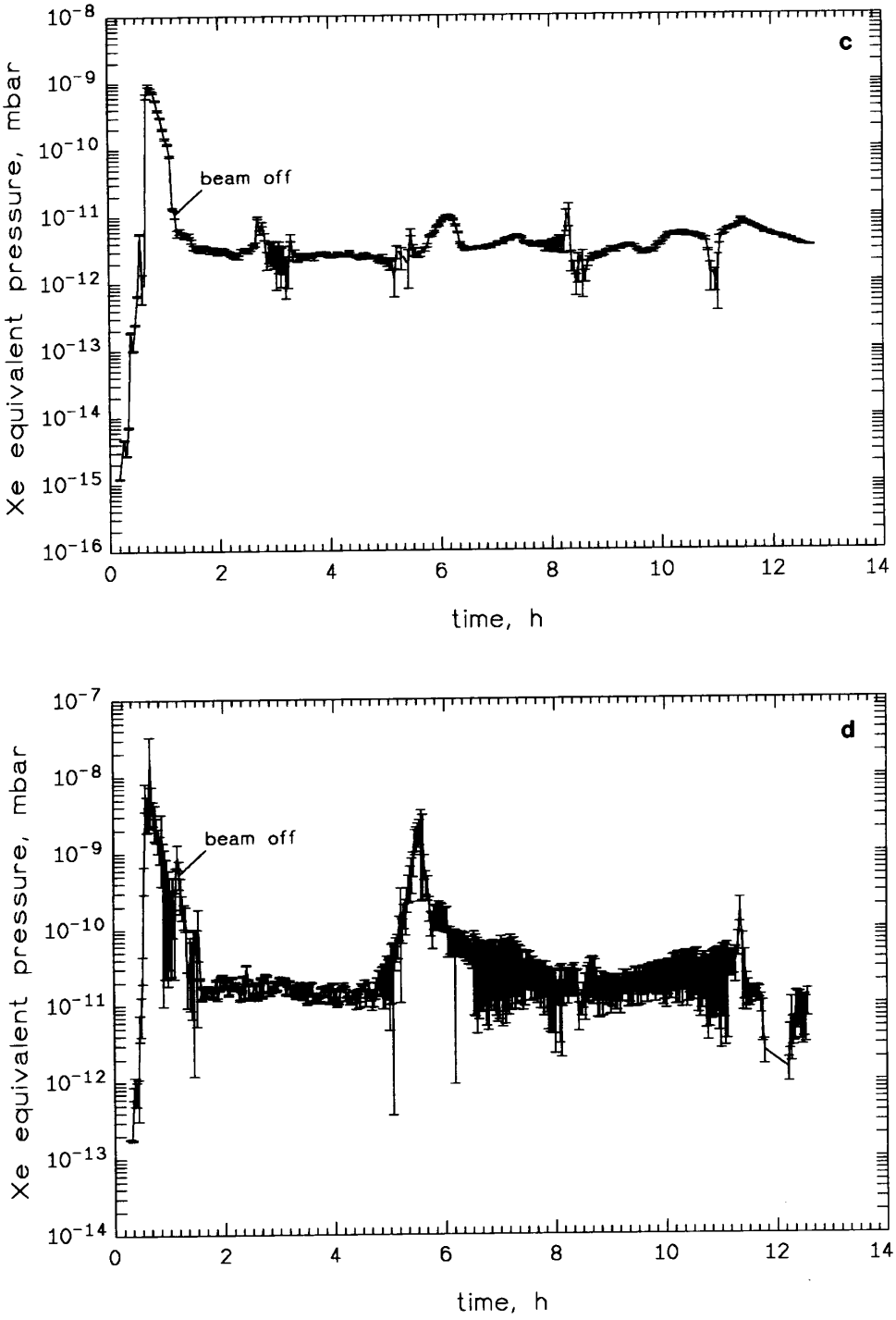

FIG. 2—*Continued*

increasing irradiation time as an indication of secondary decomposition and/or recombination via (10).

$$CH_3 \rightarrow CH_2 + H\,, \tag{8}$$

$$CD_3 \rightarrow CD_2 + D\,. \tag{9}$$

Likewise, the CD_3H feature onsets after 6 minutes irradiation time, strongly indicating that this isotopically mixed methane molecule is a secondary product formed via recombination of a methyl group with atomic deuterium:

$$CH_3 + D \rightarrow CH_3D\,. \tag{10}$$

Recombination products of reactions (11) and (12) exhibit a delayed appearance as well (here 15 and 9 minutes, respectively):

$$CH_2 + D \rightarrow CH_2D\,, \tag{11}$$

$$CD_2 + H \rightarrow CD_2H\,. \tag{12}$$

Both temporal profiles stand in strong agreement with a diffusion-controlled reaction mechanism since the expected lower diffusion coefficient of D versus H is reflected in a later onset of reaction (11) as compared to (12).

Finally, we stress that the mobility of CH_2, CD_2, CH_3, and CD_3 radicals start between 60 and 75 K, well below the maximum temperature in our LT experiments of 15 K

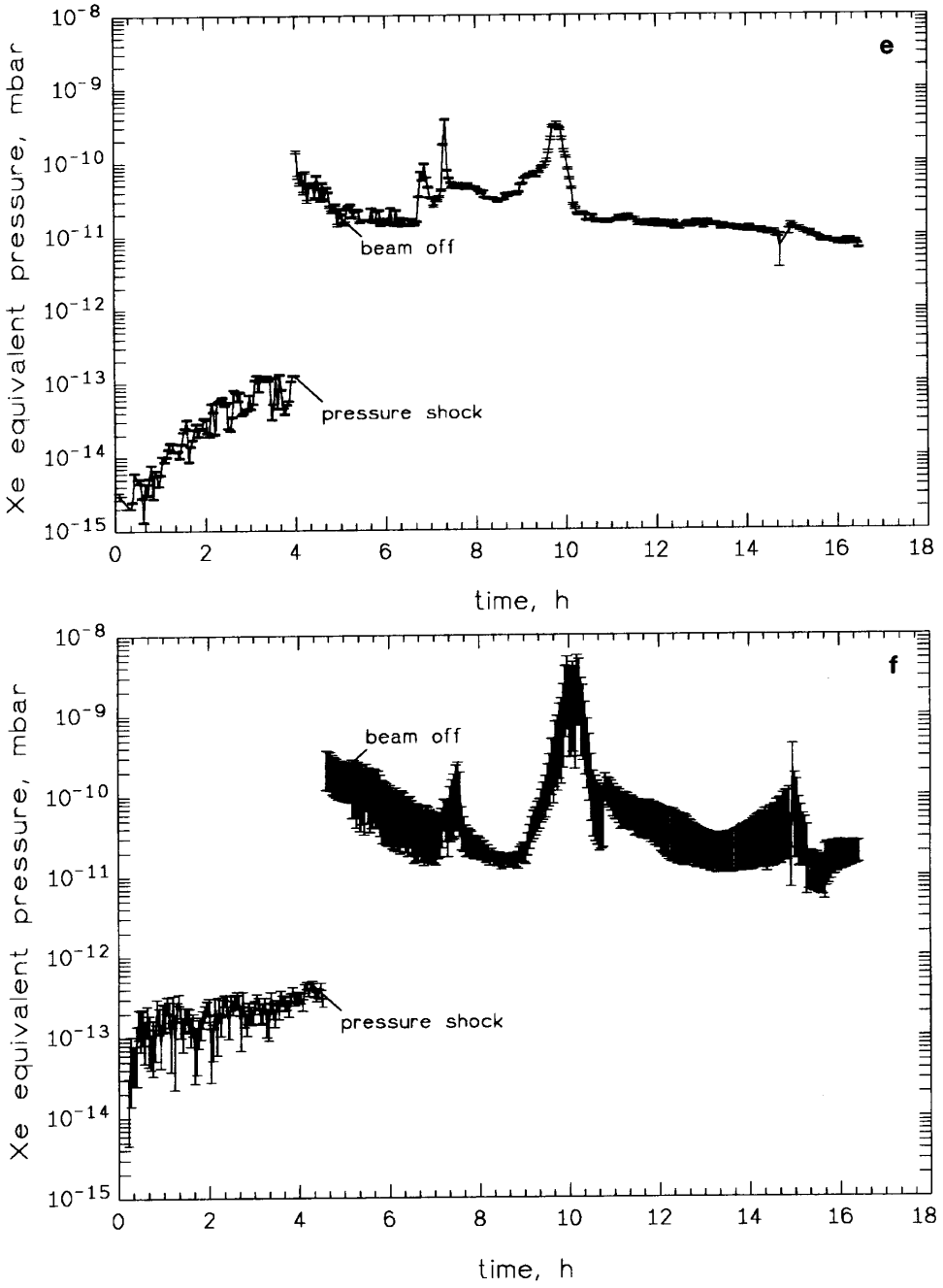

FIG. 2—*Continued*

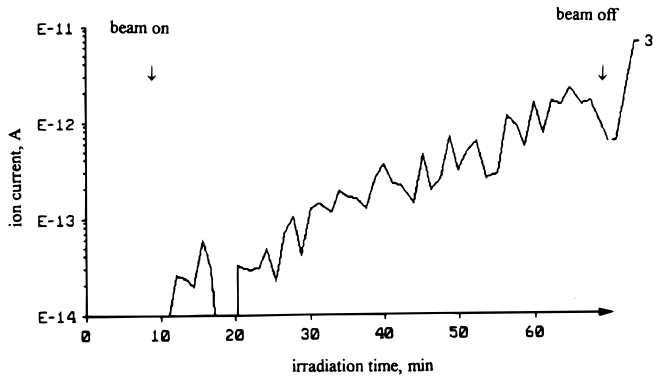

FIG. 3.—Temporal profile of HD signal upon 9 MeV α-particle ion irradiation of a CH_4/CD_4 target at 10 K.

(Kaiser et al. 1995). In strong coincidence, no isotopically mixed recombination products, $C_2H_2D_2$ ($CH_2 + CD_2$) and $C_2H_3D_3$ ($CH_3 + CD_3$), are detected either via QMS or FTIR, indicating that even reactions of neighboring carbon-containing hydrocarbon radicals are completely absent.

3.3.2. CH_4/O_2 *Targets*

As expected, FTIR spectra show absorption features of CH_3 and CH_2 radicals. Further, patterns of the hydrogenperoxy radicals (HO_2; $\nu_2 = 1409$–1395.5 cm^{-1}) as a reaction product of H atoms with nonmobile matrix-isolated O_2 via (13) appear (see Fig. 5):

$$H + O_2 \rightarrow HO_2 . \quad (13)$$

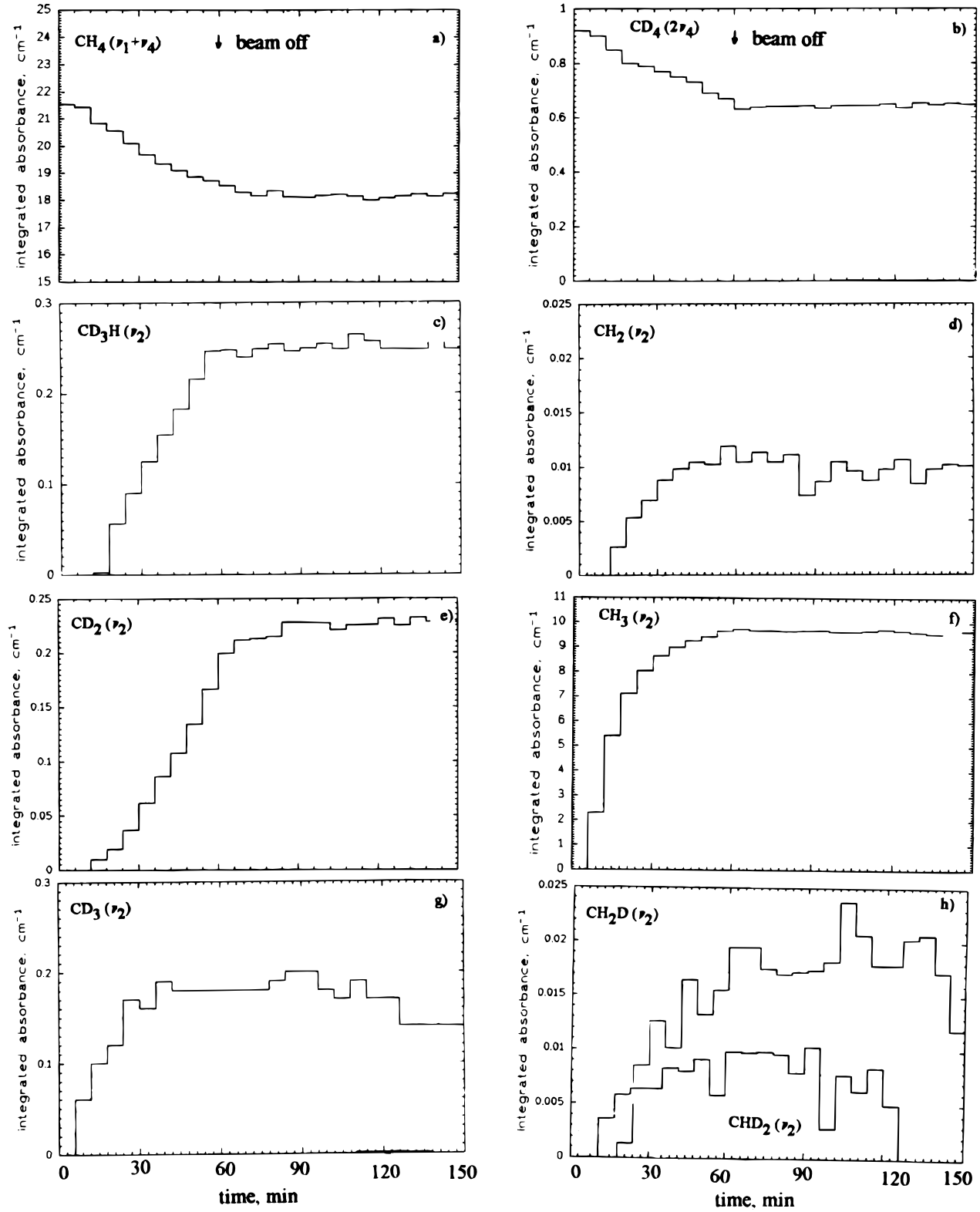

FIG. 4.—Temporal profile of CH_xD_y species upon 9 MeV α-particle ion irradiation of a CH_4/CD_4 target at 10 K

The initial linear profile reaches a maximum after about 20 minutes and drops to zero intensity after an additional 140 minutes. Since the CH_3 profile and corresponding production of H atoms is still increasing, the sequential transformation of O_2 in H_2O via equations (14)–(16) is extremely likely:

$$O_2H + H \rightarrow H_2O_2 , \quad (14)$$

$$H_2O_2 \xrightarrow{\alpha} 2HO , \quad (15)$$

$$HO + H \rightarrow H_2O . \quad (16)$$

This reaction sequence is reflected in an increasing size of OH aggregates from dimers (Fig. 6*a*), trimers (Fig. 6*b*), and tetramers (Fig. 6*c*) to polymers (Fig. 6*d*) as well.

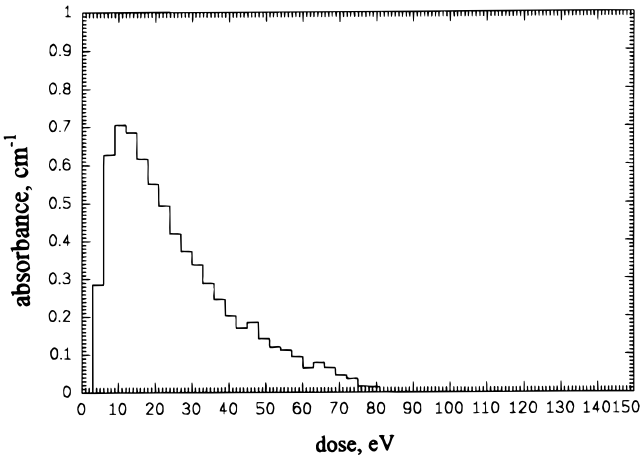

FIG. 5.—Temporal profile of O_2H radicals upon 9 MeV α-particle ion irradiation of a O_2/CH_4 target at 10 K.

3.3.3. *Target Explosions*

Figure 7 displays typical FTIR spectra before and after the explosions upon irradiation of CH_4 and CD_4 targets with 9 MeV α-particles at 10 K the absorption features of which are compiled in Tables 3 and 4. As is evident, these explosions release up to 90% of the solid target into the gas phase. The remaining residue on the silver waver consists predominantly of CH_4 and CD_4, synthesized C_2H_2, C_2H_4, C_2H_6 molecules, as well as higher alkanes containing methyl (CH_3), methylene (CH_2), and methin (CH) groups. A detailed reaction network leading to these molecules is given in a forthcoming paper (Kaiser et al. 1997).

TABLE 3

SELECTIVE ASSIGNMENT OF VIBRATION MODELS OF $^{13}CH_4$ AT 10 K

Mode	Absorption (cm^{-1})
$\nu_3 + \nu_4$.....	4283
$\nu_1 + \nu_3$.....	4193
$3\nu_4$	3825

4. DISCUSSION

4.1. *Formation of Atomic and Molecular Hydrogen*

The computer simulations and experiments reveal that formation of CH_3 and H upon MeV particle irradiation of solid CH_4 at 10 K followed by recombination of two hydrogen atoms is the key step to molecular hydrogen (see Fig. 8). Here a 9 MeV α-particle transfers part of its energy to the electronic system of the CH_4 molecule, forming an electronically excited $[CH_4]^*$. Bond cleavage yields first a radical pair $[CH_3\text{--}H]$ trapped in the surrounding methane matrix. The H atom either holds a kinetic energy large enough to overcome the diffusion barrier and separates from the radical cage or it reacts back with the neighboring methyl radical to CH_4 if the diffusion barrier cannot be passed. Since the simple Arrhenius model calculates the ratio of H and D diffusion coefficients to be $k_D(H)/k_D(D) = 1.4$, H atoms from $[CH_3\text{--}H]$ should diffuse preferentially compared to $[CD_3\text{--}D]$, and our model is expected to go hand in hand with a $[H_2]/[D_2]$ formation yield larger than 1, as verified experimentally to 6 ± 2.

To a minor amount, secondary dissociation of CH_3 to H and CH_2 contribute to form H. Similar to CH_3, CH_2 reacts with a hydrogen atom to recombine to CH_3 radicals as proven via detection of CH_2D as well as CD_2H. The H diffusion is further documented probing CH_3D as a recombination product of CH_3 and a D atom, monitoring the O_2H radical, and sampling HD. Since these reactions do not show any entrance barrier except the diffusion barrier prior to reaction, all processes are expected in interstellar ices as well. The diffusion of CH_2 and CH_3 radicals, however, starts at about 35–46 and 70 K in CH_4 and Xe matrixes (Bhattacharya & Willard 1982) and does not influence the chemistry in the present experiments. This pattern is reflected in our CH_4/O_2 experiment as well since even the barrierless reaction of CH_3 with O_2 to CH_3OO radicals could not be verified.

Besides the inelastic energy transfer, the implanted ions generate to a lesser extent (<1%) C and H knock-on atoms

TABLE 4

ABSORPTION FEATURES OF FTIR SPECTRA AS SHOWN IN FIGURE 7

Assignment	Mode (absorption) (cm^{-1})
H-^{13}C ≡ ^{13}C-R	νCH(sp)(3264, 3251, 3248, 3220)
= $^{13}CH_2$(sp^2)	νCH(3084, 3077, 3035), νC = C(1643, 1650), δ_{ip}(1417, 1419), δ_{op}(890, 897)
-$^{13}CH_3$	ν_{as}(2969, 2962, 2958), ν_s(2880), δ_{as}(1464, 1454), δ_s(1361, 1360)
-^{13}C($^{13}CH_3$)$_2$-.....	δ_s(1386, 1366) ν_3(1135), ν_4(824, 820, 816)
-$^{13}CH_2$-(sp^3).....	ν_{as}(2951, 2930), δ_b(1433)
-($^{13}CH_2$)n-$^{13}CH_3$ (n = 1, 2).....	rocking (764 n = 1; 745, n = 2)
-^{13}CH-(sp^3).....	ν(2880)
^{13}R-^{13}C ≡ ^{13}C-^{13}R′	νC ≡ C(2156, 2177, 2087, 2201)
Substituted benzenes	1030, 1028, 1026, 835, 793
$^{13}CH_2$(carbene radical)	ν_2(1108)
$^{13}CH_3$(methyl radical)	ν_2(604)
$^{13}C_2H_5$-radical	ν_9(531)
$^{13}C_2H_3$-radical	ν_7(892)
$^{13}C_2H_2$	ν_3(3261), ν_5(735)
$^{13}C_2H_4$	ν_7(956)
$^{13}C_2H_6$	ν_8(1460), ν_6(1366), ν_9(820)

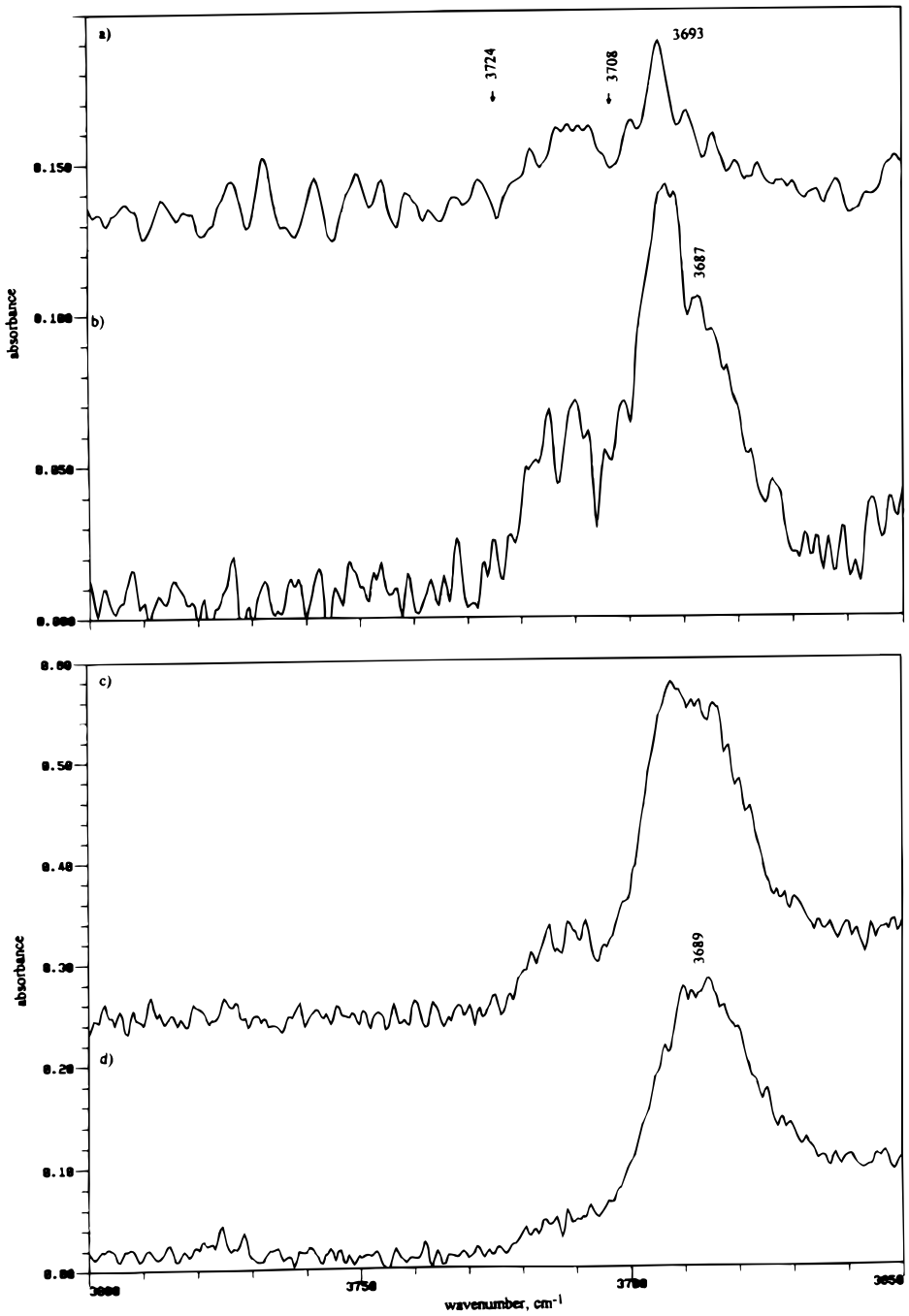

FIG. 6.—Transition from di (*a*), tri (*b*), and tetra (*c*) to polymer-like OH aggregates with increasing irradiation dose from (*a*) 6 ± 1 eV, (*b*) 12 ± 2 eV, (*c*) 45 ± 7 eV to (*d*) 90 ± 10 eV upon 9 MeV α-particle ion irradiation of a O_2/CH_4 target at 10 K.

in elastic encounters with the target atoms. Suprathermal recoils abstract H atoms, to form CH or H_2, respectively, and/or insert into chemical bonds (eqs. [5] and [6] to generate H/H_2 or simply thermalize.

4.2. *Target Explosions*

Our experimental data indicate that O_2 molecules inhibit the explosions upon irradiation of CH_4 targets with 9 MeV α-particles and scavenge mobile radicals. Since atomic hydrogen represents the only diffusing species in our LT experiments and absorption of matrix-isolated O_2H radicals were detected, these findings strongly suggest H atoms play a major role in this process. Further, our FTIR results show a leveling CH_3 concentration prior to the explosive process correlating with an equimolar formation of hydrogen atoms which recombine to H_2 or are stored inside the CH_4 target. If we calculate the limiting CH_3 radical concentration, assume an identical H profile, and correct for the H_2 released into the gas phase, we find a critical concentration of $6 \pm 3\%$ of the total hydrogen trapped as H atoms before the explosion occurs. Further radiation exposure very likely triggers a chain of H atom recombination leading to ejection of up to 90% of the total target into the gas phase. Since no H atoms are stored in the CH_4/O_2

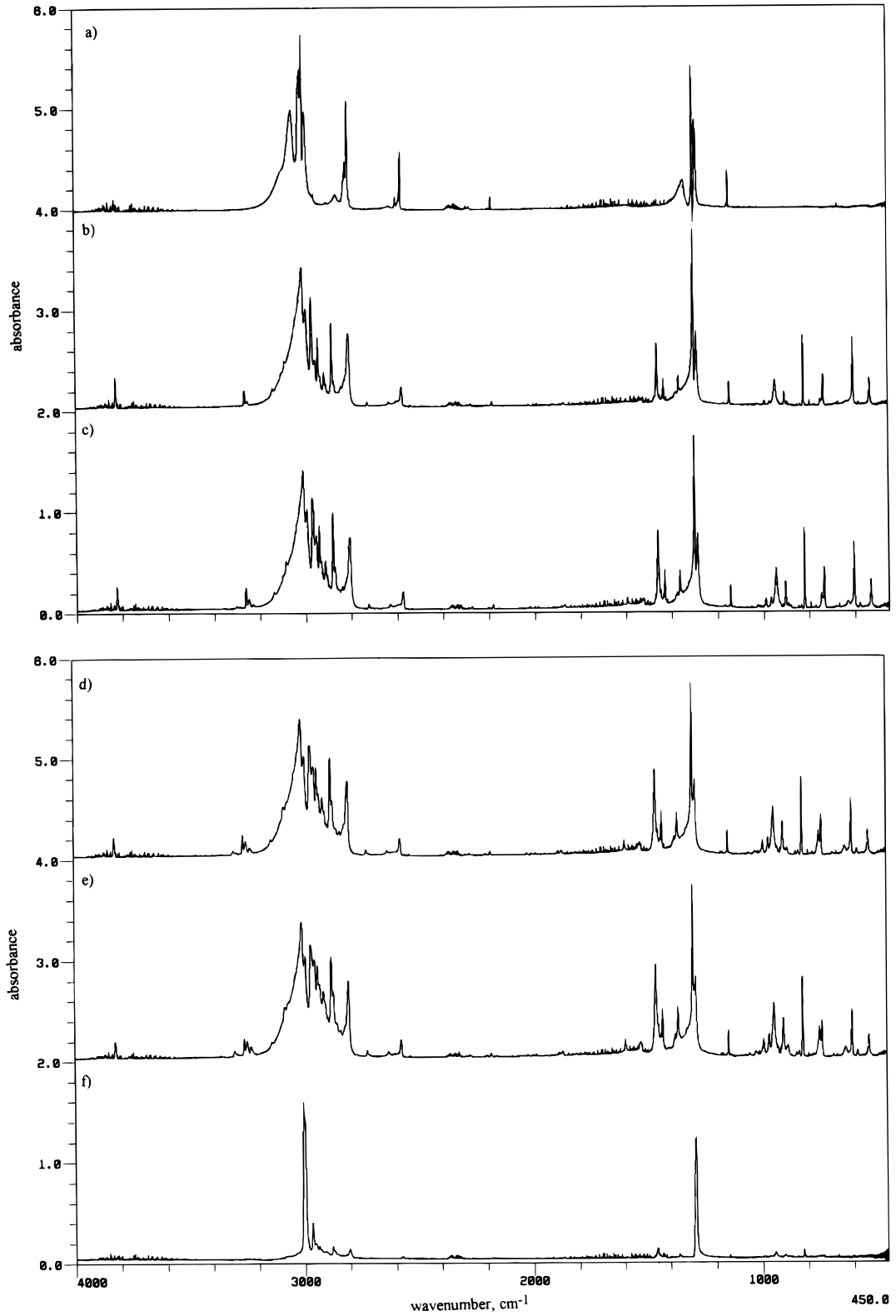

FIG. 7.—FTIR spectra of a $^{13}CH_4$ target upon 9 MeV α-particle ion irradiation at 10 K. (*a*) 0 eV; (*b*) 30 ± 3 eV; (*c*) 60 ± 6; (*d*) 90 ± 9 eV; (*e*) before the explosion; and (*f*) after the explosion.

target, no explosions are anticipated as verified experimentally. The remaining question to be solved is classification of this explosion as an equilibrium or nonequilibrium process. We tackle this question calculating the maximum energy release if all H atoms stored prior to the explosion recombine in an infinite short time interval to H_2, releasing 4.5 eV per H-H bond. But even including CH_3-CH_3 recombination can supply only about 50% of the energy required to sublime 90% of the target into the gas phase. Therefore, the explosion resembles a nonequilibrium process in which

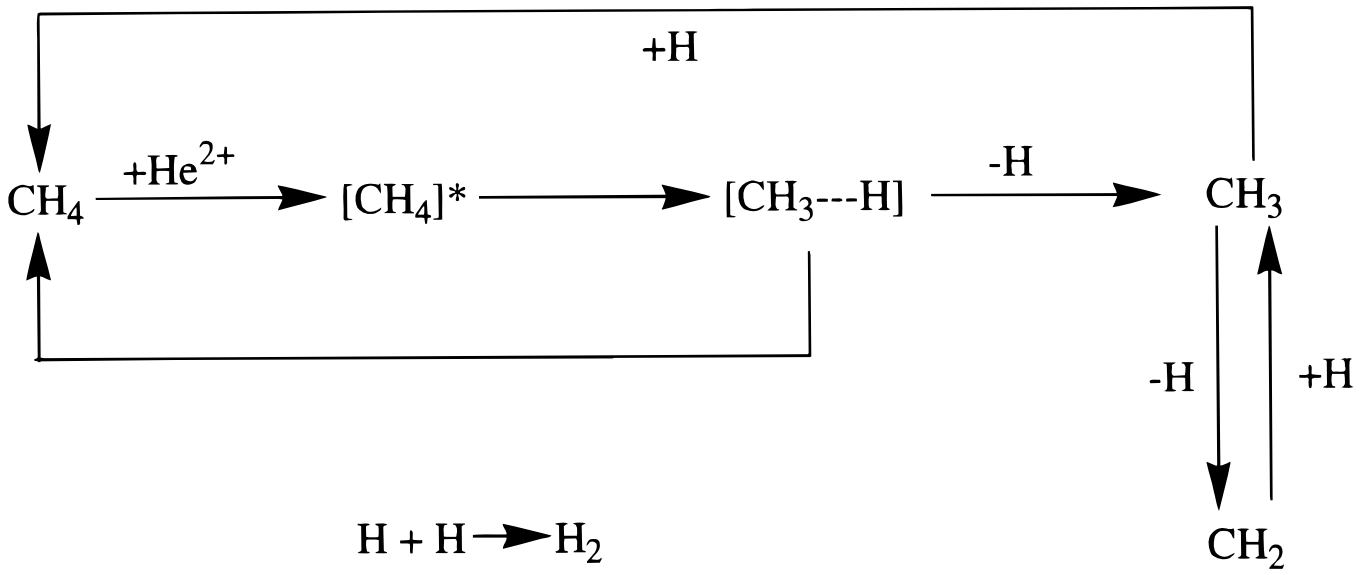

FIG. 8.—Compilation of mechanisms leading to formation of atomic and molecular hydrogen

ice chunks are transferred into the gas phase. A pure equilibrium sublimation cannot be covered energetically.

5. ASTROPHYSICAL IMPLICATIONS

Since CH_4 constitutes only about 1%–8% of all molecules such as NH_3, H_2O, CO, and CH_3OH condensed on interstellar grains, our laboratory experiments resemble model studies on the interaction of cosmic-ray particles with frozen organic molecules on interstellar grains to elucidate basis mechanisms leading to H/H_2 formation. In this final chapter, we transfer our findings to astrophysically relevant ice mixtures as well as to our own solar system.

5.1. *Physical Effects*

The detected explosions upon the ion irradiation resemble a fundamental process in the redistribution of newly formed molecules from the solid state into the gas phase even at temperatures as low as 10 K, if a critical concentration of radicals can be accumulated in the ices. Current models postulate explosive description in which the ice/grain mantle is heated sufficiently to about 24–28 K to release its chemical energy via radical recombination (Schutte & Greenberg 1991; d'Hendecourt, Allamandolla, & Greenberg 1982). Our experiments strongly indicate that temperature does not necessarily have to be an essential parameter for explosions and ejection of molecules into the gas phase, but a simple radical accumulation does this job just as well at temperatures of 10 K. These processes could resolve hitherto unresolved enrichments of long chained hydrocarbon molecules in the interstellar gas phase.

5.2. *Chemical Effects*

Our results clearly demonstrate the urgency to include cosmic-ray triggered formation of atomic as well as molecular hydrogen as an additional pathway in models simulating interstellar grain chemistry. In the interstellar medium and in regions of our solar system extending to Oort's cloud, the cosmic ray particle flux distribution is dominated by the MeV energy regime leading predominantly (>99%) to inelastic energy loss processes and production of H atoms in the initial step. This energy transfer results in bond rupture processes forming in ice mixtures not only CH_3 radicals and atomic hydrogen, but to OH and NH_2 radicals as well:

$$NH_3 \xrightarrow{\alpha} NH_2 + H\,, \tag{17}$$

$$H_2O \xrightarrow{\alpha} OH + H\,. \tag{18}$$

At first glance, interstellar and solar UV photons can photolyse NH_3 and H_2O via equations (17) and equation (18) as well. However, the typical penetration depth of a UV photon is limited to 0.2–0.5 μm, whereas MeV particles can be implanted several centimeters inside solid ices present in cometary bodies. This limits the hydrogen production zone in cometary nuclei stored in Oort's cloud not only to the surface but inside their interior as well. Further, a photolyses via reactions (17) and (18) proceeds in a one-photon step, whereas a single MeV particle can generate up to 10^5 radical pairs. This order of magnitude alone urges the need to incorporate cosmic-ray–induced CH_3, OH, and NH_2 radical productions in models of interstellar grains as well as cometary chemistry as additional pathways to reactive species stored ice matrices besides photolyses.

Besides the initial H formation, thermal and suprathermal hydrogen atoms are expected to show an even more profound effect on the chemistry of interstellar and planetary ices. Suprathermal hydrogen can overcome barriers to H abstraction ranging between 30 and 80 kJ mol^{-1} to form H_2 and open shell radicals:

$$H + CH_4 \rightarrow H_2 + CH_3\,, \tag{19}$$

$$H + C_2H_6 \rightarrow H_2 + C_2H_5\,, \tag{20}$$

$$H + H_2O \rightarrow H_2 + OH\,, \tag{21}$$

$$H + NH_3 \rightarrow H_2 + NH_2\,. \tag{22}$$

Likewise, H atoms add to triple and double bonds of grain molecules of, e.g., CO, H_2CO, C_2H_2, and C_2H_4; the reactions with CO and H_2CO are especially of fundamental interest as they are postulated to account for formation of interstellar methanol on grains. The N_2 reaction to N_2H as well as the barrierless encounter of H and O_2 to form O_2H might help to identify N_2/O_2–containing molecules. Thermal hydrogen atoms react as well, but the reactions are anticipated to hold rate constants several orders of magnitude lower since these processes proceed via tunneling (Dubinskaya 1978; Hiraoka et al. 1994, 1995). Prospective models of interstellar grain or planetary chemistry must account for these elementary reactions.

In strong contrast to the H atom reactions, however, addition of CH_3 radicals to unsaturated molecules is irrelevant at typical grain temperatures between 10 and 100 K since the barriers of about 100 kJ mol^{-1} are energetically not accessible. In addition, the mass of 15 amu of the methyl group as compared to 1 amu of atomic hydrogen rules out tunneling processes. Further, H atoms diffuse long distances and might react with atoms trapped on grain surfaces to form CH, NH, and OH radicals (Tielens & Allamandola 1987). If adsorbed metal atoms react as well, this process might supply metal hydrides accumulated on interstellar grains and depleted from the gas phase (Wetly et al. 1995).

Finally, experimentally found isotope effects based on preferential diffusion of lighter H atoms versus D strongly suggest a deuterium isotope enrichment on interstellar grain material and hydrocarbon-rich ices in our solar system. In our solar system, solid CH_4 has been detected on Triton, Uranus, Neptune, Pluto and its moon Charon, and isotope enrichments are expected. Further space missions and observations should especially focus on the CH_4 to CH_3D ratio: an increased CH_3D concentration deviating from thermal equilibrium predications might indicate reaction (10) takes over. Likewise, enhanced HDO/H_2O and NH_2D/NH_3 ratios are expected as well.

The authors want to thank the cyclotron crew of the compact cyclotron CV 28 at the Forschungszentrum Jülich for performing the irradiation and G. Stöcklin, director of Institut für Nuklearchemie, for his invaluable assistance with financing the experimental setup. One of us, R. I. K., is indebted to the Deutsche Forschungsgemeinschaft (DFG) for financial support to present parts of this work on Radiation-Effects in Insulators (REI-7, Nagoya, Japan) and to B. Krebs, Westfälische Wilhelms Universität Münster, for administrative guidance and advice.

REFERENCES

Becker, R. S., Hong, K., & Hong, H. 1974, J. Mol. Evol., 4, 157
Bhattacharya, D., & Willard, J. E. 1982, J. Phys. Chem., 86, 962
Brown, W. L., Foti, G., Lanzerotti, L. J., Bower, J. E., & Johnson, R. E. 1987, Nucl. Instrum. Methods Phys. Res., 19/20, 899
d'Hendecourt, L. B., Allamandolla, L. J., & Greenberg, J. M. 1985, A&A, 152, 130
Dubinskaya, A. M. 1978, Russian Chem. Rev., 47, 614
Grigorev, E. I., Slavinskaya, N. A., Pshezhetskii, S. Y., & Trakhtenberg, L. I. 1988, Khimiya Vysokikh Energii, 22, 31
Hauge, E. H., & Stovneng, J. A. 1989, Rev. Mod. Phys., 61, 917
Hiraoka, K., Ohaski, N., Kihara, Y., Yamamoto, K., Sato, T., & Yamashita, A. 1994, Chem. Phys. Lett., 229, 408
Hiraoka, K., Yamashita, A., Yachi, Y., Aruga, K., Sato, T., & Muto, H. 1995, ApJ, 443, 363
Johnson, R. E. 1996, Rev. Mod. Phys., 68, 305
Johnson, R. E., Brown, W. L., & Lanzerotti, L. J. 1983, J. Phys. Chem., 87, 4218
Kaiser, R. I., Eich, G., Babrysch, A., & Roessler, K. 1997, ApJ, submitted
Kaiser, R. I., Gabrysch, A., & Roessler, K. 1995a, Rev. Sci. Instrum., 66, 3058
Kaiser, R. I., Jansen, P., Petersen, K., & Roessler, K. 1995b, Rev. Sci. Instrum., 66, 5226
Kaiser, R. I., & Roessler, K. 1997, ApJ, 475, 1144
Pironello, V. 1991, in Chemistry in Space, ed. D. M. Greenberg & V. Pironello (Dordrecht: Kluwer), 263
Pironello, V., & Averna, D. 1988, in Experiments on Cosmic Dust Analogues (Dordrecht: Kluwer), 281
Pironello, V., Brown, W. L., Lanzerotti, L. J., & MacLennan, C. G. 1988, Experiments on Cosmic Dust Analogues (Dordrecht: Kluwer), 287
Robinson, M. T. 1992, Nucl. Instrum. Meth., B67, 396
Roessler, K. 1992, in Handbook of Hot Atom Chemistry, ed. D. P. Adloff et al. (Tokyo/Weinheim: Kodansha), 265
Romani, P. N., & Atreya, S. K. 1988, Icarus, 74, 424
Sandford, S. A., & Allamandola, L. J. 1993, ApJ, 409, L65
Schutte, W. A., & Greenberg, J. M. 1991, A&A, 244, 190
Smoluchowski, R. 1981, Ap&SS, 75, 3553
Tielens, A. G. G. M., & Allamandola, L. J. 1987, in Interstellar Processes (Dordrecht: Reidel), 397
Trakhtenberg, L. I., & Milikh, G. M. 1982, Khimiya Vysokikh Energii, 17, 483
Welty, D. E., Hobbs, L. M., Lauroesch, J. T., Morton, D. C., & York, D. G. 1995, ApJ, 449, L135